Overexpression of Slit2 improves function of the paravascular pathway in the aging mouse brain

GE LI[1*], XIAOFEI HE[2*], HANG LI[1], YU'E WU[1], YALUN GUAN[1], SHUHUA LIU[1], HUANHUAN JIA[1], YUNFENG LI[1], LIJING WANG[3], REN HUANG[1], ZHONG PEI[2], YUE LAN[4] and YU ZHANG[1]

[1]Guangdong Provincial Key Laboratory of Laboratory Animals, Guangdong Laboratory Animals Monitoring Institute, Guangzhou, Guangdong 510663; [2]Department of Neurology, National Key Clinical Department and Key Discipline of Neurology, Guangdong Key Laboratory for Diagnosis and Treatment of Major Neurological Diseases, The First Affiliated Hospital, Sun Yat-sen University, Guangzhou, Guangdong 510080; [3]Vascular Biology Research Institute, School of Basic Course, Guangdong Pharmaceutical University, Guangzhou, Guangdong 510006; [4]Department of Rehabilitation Medicine, Guangzhou First People's Hospital, Guangzhou Medical University, Guangzhou, Guangdong 510180, P.R. China

Received December 28, 2017; Accepted July 24, 2018

DOI: 10.3892/ijmm.2018.3802

Abstract. Aging is associated with impairment of the paravascular pathway caused by the activation of astrocytes and depolarization of protein aquaporin-4 (AQP4) water channels, resulting in the accumulation of protein waste, including amyloid β (Aβ), in the brain parenchyma. The secreted glycoprotein slit guidance ligand 2 (Slit2) is important in regulating the function of the central nervous system and inflammatory response process. In the present study, 15-month-old Slit2 overexpression transgenic mice (Slit2-Tg mice) and two-photon fluorescence microscopy were used to evaluate the dynamic clearance of the paravascular pathway and the integrity of the blood-brain barrier (BBB). The reactivity of astrocytes, polarity of AQP4 and deposition of Aβ in the brain parenchyma were analyzed by immunofluorescence. A Morris water maze test was used to examine the effect of Slit2 on spatial memory cognition in aging mice. It was found that the overexpression of Slit2 improved the clearance of the paravascular pathway by inhibiting astrocyte activation and maintaining AQP4 polarity on the astrocytic endfeet in Slit2-Tg mice. In addition, Slit2 restored the disruption of the BBB caused by aging. The accumulation of Aβ was significantly reduced in the brain of Slit2-Tg mice. Furthermore, the water maze experiment showed that Slit2 improved spatial memory cognition in the aging mice. These results indicated that Slit2 may have the potential to be used in the prevention and treatment of neurodegenerative diseases in the elderly.

Correspondence to: Professor Yu Zhang, Guangdong Provincial Key Laboratory of Laboratory Animals, Guangdong Laboratory Animals Monitoring Institute, 11 Fengxin Road, Guangzhou Science City, Guangzhou, Guangdong 510663, P.R. China
E-mail: zhy@gdlami.com

Professor Yue Lan, Department of Rehabilitation Medicine, Guangzhou First People's Hospital, Guangzhou Medical University, 1 Panfu Road, Guangzhou, Guangdong 510180, P.R. China
E-mail: bluemooning@163.com

*Contributed equally

Key words: slit guidance ligand 2, paravascular pathway, astrocyte, aquaporin-4, amyloid β, spatial memory cognition

Introduction

The accumulation of amyloid β (Aβ) is a histopathological hallmark of Alzheimer's disease (AD) (1). Substantial evidence suggests that astroglial-mediated interstitial fluid (ISF) bulk flow, known as the paravascular pathway, may contribute to a large portion of Aβ clearance (2,3). In the paravascular pathway, subarachnoid cerebrospinal fluid (CSF) driven by vasomotion rapidly recirculates through the brain along paravascular spaces surrounding cerebral arteries. ISF and interstitial solutes are cleared through the paravascular spaces surrounding cerebral veins (2,4,5). The astroglial water channel protein aquaporin-4 (AQP4) is key in the paravascular pathway (2). AQP4 deficiency or dysfunction significantly impairs the function of the paravascular pathway. In the aging brain, the function of AQP4 decreases due to the increasing reactivity of astrocytes, thereby leading to a 40% reduction in Aβ clearance by the paravascular pathway (3).

The secreted glycoprotein slit guidance ligand 2 (Slit2) was first identified as an axonal repellent in the development of the central nervous system (CNS) through interaction with four cognate roundabout (Robo) receptors, Robo1-4 (6). The interactions between Slit2 and its receptors is context dependent, creating a multifunctional platform for cell-cell or cell-matrix interactions, impacting cell migration, polarity and adhesion (7). Slit2 has been reported to have beneficial and detrimental effects in diseases of the brain. For example, in the ischemic brain, Slit2 is secreted by astrocytes as an autocrine

or paracrine molecule interacting with Robo, which reduces immune cell recruitment to ischemic tissue and mediates neuroprotection (8). The function of Slit2 in neuro-inflammation is closely associated with reactive astrocytes (9). By contrast, the overexpression of Slit2 increases the permeability of the blood brain barrier (BBB), which is associated with AD-like alterations in animals (10,11). As disruption of the BBB and inflammation are closely linked to aging-related neurodegenerative disease (12,13), it is necessary to examine the role of Slit2 in the pathogenesis of neurodegenerative diseases.

In the present study, using Slit2 overexpression transgenic mice (Slit2-Tg mice), the role of Slit2 in maintaining the function of the paravascular pathway in the aging mouse brain was evaluated, and the effects of Slit2 on reducing the risk of neurodegenerative diseases were examined.

Materials and methods

Animals. All animal experiments in the present study were approved by the Institutional Animal Care and Use Committee of Guangdong Laboratory Animals Monitoring Institute (Guangzhou, China; IACUC no. 2015023). All procedures were performed in accordance with the AAALAC guidelines (14).

The Slit2-Tg mice overexpressing human Slit2 were from Guangdong Pharmaceutical University (Guangzhou, China), as previously described (15). The heterozygous transgenic mice were crossed with C57BL/6 mice (Stock no. 000664; Jackson Laboratory, Ben Harbor, ME, USA) to generate Slit2-Tg mice and wild-type littermates (WT mice). Unless otherwise noted, the animals used in the present study defined as aging were 15-month-old adult male mice. All mice were provided with water and a standard chow diet *ad libitum*. The mice were housed in a specific pathogen-free facility with a 12 h light/dark cycle at 23±2˚C and 50±10% humidity.

The transgenic offspring were identified by polymerase chain reaction (PCR) using the following primer sequences: Slit2 forward 5'-CCCTCCGGATCCTTTACCTGTCAAGGTCCT-3' and Slit2 reverse 5'-TGGAGAGAGCTCACAGAACAAGCCACTGTA-3' (Invitrogen; Thermo Fisher Scientific, Inc., Waltham, MA, USA); the product size was 645 bp. In all experiments, the animals were anesthetized with chloral hydrate (4.2%, 0.01 ml/g).

Reverse transcription-quantitative PCR (RT-qPCR) analysis. Following CO_2 euthanasia, mouse brains were removed and total RNA extraction using TRIzol (Invitrogen; Thermo Fisher Scientific, Inc.) and RT was performed using the PrimeScript™ RT reagent kit (Takara Bio, Inc., Otsu, Japan) at 37˚C for 30 min and 85˚C for 1 min, according to the manufacturer's protocol. The primers used for Slit2 were provided by Invitrogen; Thermo Fisher Scientific, Inc. and were as follows: Forward, 5'-AGCCGAGGTTCAAAAACGAGA-3' and reverse, 5'-GGCAGTGCAAAACACTACAAGA-3' (Invitrogen; Thermo Fisher Scientific, Inc.). The qPCR analysis was performed as follows: 95˚C for 30 sec followed by 40 cycles of 95˚C for 5 sec and 60˚C for 34 sec, using an ABI-7500 Fast Real-Time PCR system (Applied Biosystems; Thermo Fisher Scientific, Inc.) in a total volume of 25 μl containing 2 μM primers, 80 μg cDNA and 12.5 μl of the SYBR® Premix Ex Taq™ (Takara Bio, Inc.). The results were quantified using the $2^{-\Delta\Delta Cq}$ method (16).

In vivo 2-photon fluorescence imaging. The fluorescent CSF tracer penetrating into the intact living brain was visualized through a closed cranial window using a custom-built 2-photon laser scanning microscope (Leica Microsystems GmbH, Wetzlar, Germany), as described previously (17,18). Briefly, the animals were anesthetized and securely placed on a stereotaxic device with the skull level between the bregma and lambda. The stereotaxic coordinates of the right parietal cortex were 2 mm caudal from the bregma, and 1.7 mm lateral from the midline (19). A thin cranial window over the parietal area was prepared for 2-photon *in vivo* imaging. As described by Ren *et al* (20), FITC-conjugated dextran (40 kDa; D-1841; Thermo Fisher Scientific, Inc.) was first reconstituted with artificial CSF into a concentration of 0.5%. This was injected it into the subarachnoid CSF via cisterna magna puncture at a rate of 2 μl/min for a period of 5 min with a microsyringe pump controller, following which 200 μl of dextran rhodamine B (70 kDa; D-1841; Thermo Fisher Scientific, Inc.) was injected intravenously immediately prior to imaging to visualize the vasculature. The mice were immediately transferred to the Leica DM6000 CFS stage (Leica Microsystems GmbH) and their head immobilized.

Imaging was performed using a Leica SP5 2-photon imaging system (Leica Microsystems GmbH) equipped with a Ti:Sapphire laser (Coherent Chameleon Ultra II; Coherent, Inc., Santa Clara, CA, USA) and 25X/0.95 NA water-immersion objective and controlled with Leica LAS X 3.3.0 software (Leica Microsystems GmbH). Images of the cerebral vasculature were first captured with 512x512 pixel frames from the surface to a depth of 300 μm with 2-μm z-steps, to avoid the influence of laser irradiation. Quantification of the mean pixel intensity of the tracer was processed from 40 μm (xyz) of the 3-dimensional image stacks obtained 5, 15, 30, 45, and 60 min following intra-cisternal injection. To examine the dissipation of tracer in the paravascular space of penetrating arterioles, the 2-photon *in vivo* image of 100-μm below the surface was captured. Donut-shaped region of interests (ROIs) were defined and the mean pixel intensity of the tracer within these ROIs in the paravascular space was quantified. The para-arteriolar ROIs at each time point in each animal were separately averaged to generate values for a single parameter.

Immunofluorescence. For histological evaluation, the mice were transcardially perfused with 50 ml of ice-cold saline followed by 200 ml of 4% (w/v) formaldehyde in PBS. The brains were removed, immersed in 20-30% sucrose solution overnight and embedded in Tissue-Tek Optimal Cutting Temperature compound (Sakura Finetechnical, Co., Ltd., Tokyo, Japan) at -20˚C. Brain tissue blocks were consecutively cryosectioned into 10-μm thick cross sections with a cryostat microtome (Leica Microsystems GmbH).

For immunofluorescence staining, the frozen sections were treated with 0.3% triton and 10% anti-donkey serum (Abcam, Cambridge, UK) for 1 h at room temperature. Subsequently, the sections were incubated overnight at 4˚C in the dark with the following primary antibodies: Mouse anti-glial fibrillary acidic protein (GFAP; cat. no. MAB360), rabbit anti-AQP4 (cat. no. AB3068), mouse anti-Aβ1-40 (cat. no. MABN11), rabbit anti-Aβ1-42 (cat. no. AB5078P; all 1:500; EMD Millipore, Billerica, MA, USA). Alexa Fluor®

488-conjugated immunoglobulin G (heavy and light chain), $F(ab)_2$ Fragment antibodies were used as secondary antibodies and incubated with the membrane at 37˚C for 1 h in the dark. These secondary antibodies were anti-mouse (cat. no. 4409) for GFAP, anti-rabbit (cat. no. 4412) for AQP4 and Aβ1-40, and anti-rabbit (cat. no. 4413; all 1:300; Cell Signaling Technology, Inc., Danvers, MA, USA) for Aβ1-42. All sections were mounted with DAPI as a nuclear stain. A Leica TCS SP5 Spectral one-photon microscope (Leica Microsystems GmbH) was used to acquire immunofluorescent staining data. The excitation powers were 5 mW for IgG Alexa Fluor 488 and 0.1 mW for IgG Alexa Fluor 555. The photomultiplier tube value was 800 V without offset. All immunofluorescence staining was repeated three times. All images were captured at the same exposure time.

Quantitative analysis for polarization of AQP4 water channel. The polarization of astrocytic AQP4 was evaluated in accordance with a previous study (21). The color channels in the histological sections labeled for GFAP and AQP4 were separated, and each image was uniformly captured at two levels (high and a low stringency thresholds). The low-stringency threshold defined the overall area of AQP4-immunoreactivity, whereas the high-stringency threshold defined the area of intense AQP4-immunoreactivty that was localized to perivascular endfeet. The ratio of the low stringency area:high stringency area was defined as 'AQP4 polarity'. A higher AQP4 polarity represented a greater proportion of immunoreactivity restricted to perivascular regions, whereas a lower proportion indicated that the distributed immunoreactivity was between the perivascular endfeet and the soma.

Morris water maze. The Morris water maze experiment was performed according to the protocols in a previous report by our group (17). The investigators were blinded during the experiment. The maze consisted of a circular tub (120 cm in diameter, 50 cm in height) and a white circular platform (10 cm). The tub was surrounded by a curtain, which was located ~1 m from the tub wall and painted with distinct geometric cues, the water (24±1˚C) was rendered opaque with white tempera paint to conceal the platform. Over 4 consecutive days, the platform was submerged 1 cm under the surface of the water in the center of one of the pool quadrants. The mice were subjected to four trials (up to 60 sec) per day from each of the four start locations. Animals that failed to locate the platform within the allotted 60 sec were gently guided to the platform. All mice remained on the platform for 10 sec at the end of each trial. On day 5, the platform was removed and a single 60 sec probe trial was performed. The swim paths were recorded using an overhead video camera and tracked by ANY-maze 6.0 (San Diego Instruments, San Diego, CA, USA). The velocity during the probe trial, the number of times the target area (former platform) was crossed and the time spent in each quadrant during the probe trial were recorded.

Statistical analysis. All data are presented as the mean ± standard deviation or standard error of the mean. An independent sample t-test or Wilcoxon rank sum test was used for comparison between two groups. One-way analysis of variance (ANOVA) or Kruskal-Wallis test and LSD t-test or Bonferroni test were used for comparison of mean pixel intensity with the PVS and the latency to the platforms during the water maze training. SPSS 20.0 (IBM SPSS, Armonk, NY, USA) software was used for the statistical analysis. Images and sections were analyzed by an investigator, who was blinded to the experimental conditions. ImageJ 1.50i (National Institutes of Health, Bethesda, MD, USA) software was applied for analysis of the immunohistochemical results. The histology data were analyzed according to a previous study (22). Briefly, four locations per sample (three fields per section; six sections per mouse) were used for analysis. Differences in fluorescent CSF tracer, perivascular GFAP and polarization of AQP4, Aβ1-40 and Aβ1-42 immunofluorescence between the Slit2-Tg mice and WT mice were compared using an unpaired t-test. Differences in the Morris water maze results were evaluated by one-way ANOVA followed by Tukey's post hoc test for multiple comparisons. $P<0.05$ was considered to indicate a statistically significant difference.

Results

Overexpression of Slit2 restores the function of the paravascular pathway in the aging brain. Impairment of paravascular pathway function in the aging brain has an adverse effect on glymphatic CSF recirculation (3). To investigate the effect of Slit2 on paravascular pathway function in the aging brain, the present study verified whether Slit2 was expressed in the mouse brain using RT-qPCR analysis, the results of which showed the overexpression of Slit2 in the brain of the Slit2-Tg mice, compared with the WT mice (Fig. 1A). Following this, the dynamics of the paravascular CSF-ISF exchange *in vivo* were evaluated by 2-photon microscopy and the intra-cisternal injection of fluorescent CSF tracer (FITC-conjugated dextran, MW 40 kDa). The cerebral vasculature was visualized through a thinned-skull window over the parietal area following caudal vein injection of Rhodamine B. As shown in Fig. 1B, the intra-cisternal injection of FITC tracer was followed by a distinct paravascular influx, which moved rapidly into the cortex along penetrating arterioles and entered the interstitium of the parenchyma. One-way ANOVA indicated that the quantification of mean pixel intensity of the 3D image stacks (Fig. 1C) was significantly different at different time points in the WT group ($F=9.927$, $P<0.001$). The LSD-t test showed that interstitial accumulation of the tracer appeared in the parenchyma within 5 min (29.22±12.53) and increased at 15 min (31.34±3.65), although there was no significant difference from that at 5 min ($P>0.05$). The mean pixel intensity of the CSF tracer peaked at ~30 min (58.50±5.66, $P<0.001$) following injection in the aging WT mice, and gradually reduced at 45 min (45.84±8.85, $P<0.05$) and at 60 min (41.16±4.41, $P>0.05$). In the Slit2-Tg mice, interstitial accumulation of the CSF tracer was also observed within 5 min (41.11±12.66), and peaked at ~15 min (60.75±6.90). Subsequently, the mean pixel intensity was significantly decreased at 30 min (39.73±7.77), 45 min (32.60±4.98) and 60 min (19.61±5.22). However, one-way ANOVA indicated that the mean pixel intensities were not significantly different from each other ($F=1.385$, $P>0.05$). The independent sample t-test indicated no significant difference in the pixel intensity at 5 min post-CSF tracer injection ($t=1.492$, $P>0.05$) or between the peak pixel intensity of the

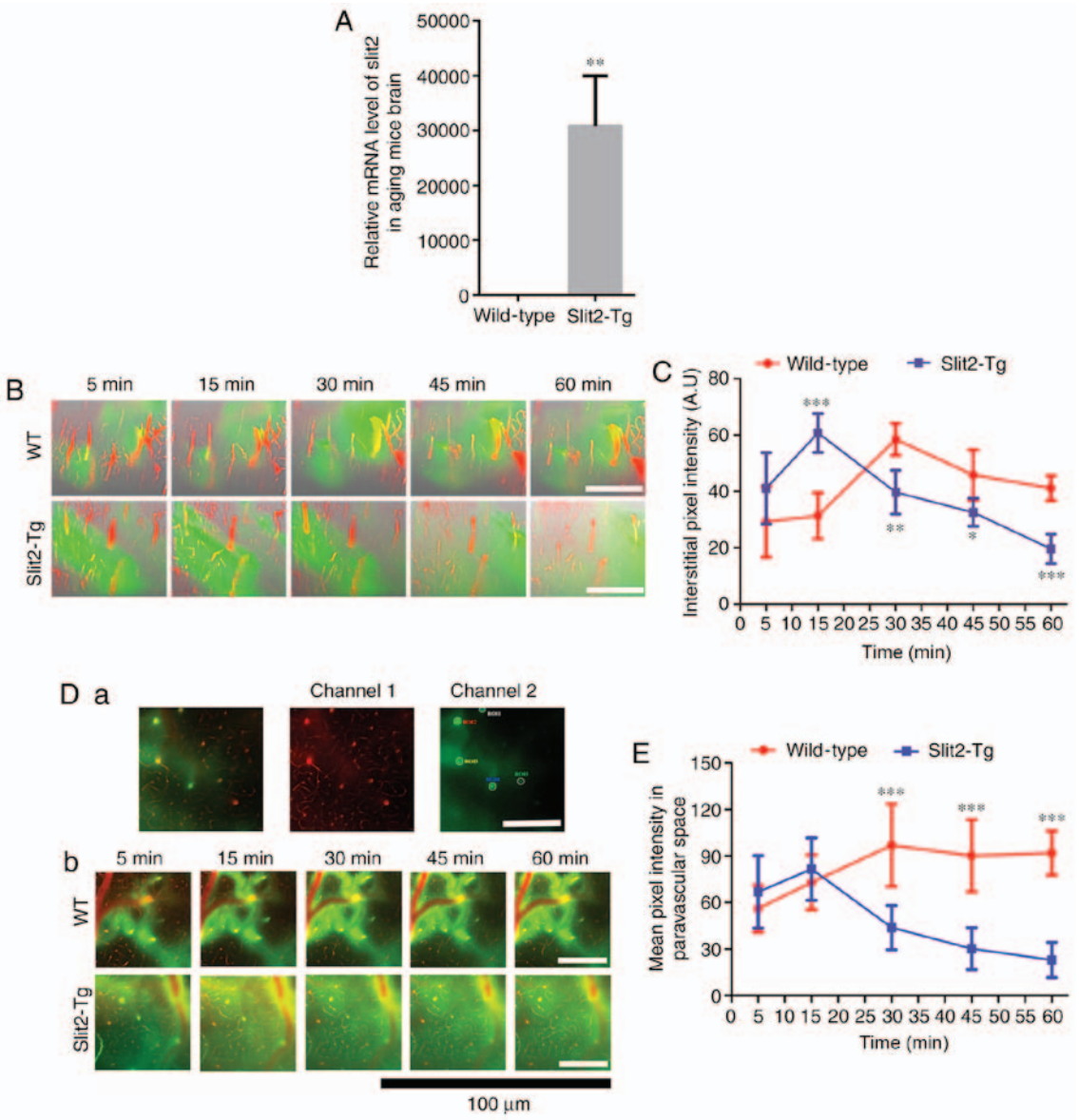

Figure 1. *In vivo* 2-photon imaging revealing Slit2 ameliorates paravascular glymphatic CSF recirculation in aging mice. (A) Relative mRNA level of Slit2 in the brain of Slit-Tg and WT mice. (B) 3D image stacks of CSF tracer penetration into the mouse cortex revealed by *in vivo* 2-photon microscopy following intra-cisternal injection of FITC-conjugated dextran (green, 40 kDa). Cerebral vasculature was visualized by intravenous injection of dextran rhodamine B (red, 70 kDa). Magnification, x250; scale bar=250 μm. (C) Quantitative analysis of the mean pixel intensity of the tracer in the 3D image stacks. (D) Accumulation of CSF tracer along perivascular spaces penetrating into the brain parenchyma, evaluated by *in vivo* 2-photon microscopy (a) region of interest used for analysis (magnification, x250; scale bar=250 μm); (b) dynamic change of CSF tracer around perivascular spaces in WT and Slit2-Tg mice (magnification, x750; scale bar=100 μm). (E) quantitative analysis of the fluorescence intensity of the CSF tracer. Each value is expressed as the mean ± standard deviation (*P<0.05, **P<0.01 and ***P<0.001, vs. Slit-Tg group; n=6 per group.). Slit2, slit guidance ligand 2; CSF cerebrospinal fluid; Tg, transgenic; WT, wild-type.

CSF tracer between the WT mice and Slit2-Tg mice (t=0.563, P>0.05). However, there was significant attenuation of the pixel intensity of CSF tracer accumulation in the parenchyma of the Slit2-Tg mice compared with that in the WT mice at 45 min (t=2.917, P<0.05) and 60 min (t=7.051, P<0.001).

The CSF tracer was analyzed in the perivascular space of penetrating arteries 100 μm below the cortical surface (Fig. 1D-a). In the aging brain of the WT mice, one-way ANOVA indicated that the accumulation of CSF tracer along perivascular spaces was significantly different at different time points (F=8.643, P<0.001). The LSD-test showed that the CSF tracer penetrating into the brain parenchyma was observed within 5 min (56.03±15.18), increased at 15 min (72.98±17.68, P<0.05) and peaked at 30 min (96.98±26.53) (Fig. 1D-b and E, P<0.01). No significant decrease in the fluorescence intensity of the CSF tracer was observed at 45 min (90.20±23.20; t=0.667, P>0.05) or 60 min (91.67±14.27). By contrast, the Kruskal-Wallis test indicated that the accumulation of CSF tracer along perivascular spaces was significantly different at different time points in the Slit2-Tg mice (P<0.001). It was present at 5 min (66.83±23.36), but decreased at 15 min (49.89±20.43) (Fig. 1D-b and E). The fluorescence intensity of CSF tracer in the paravascular space gradually decreased at 30 min (34.60±15.29), 45 min (30.21±13.48) and 60 min (22.96±11.36). Notably, the peak intensity of CSF tracer in the WT mice was significantly higher than that in the Slit2-Tg mice (t=0.243, P<0.001). An independent t-test showed that the fluorescence intensity of the CSF tracer was significantly

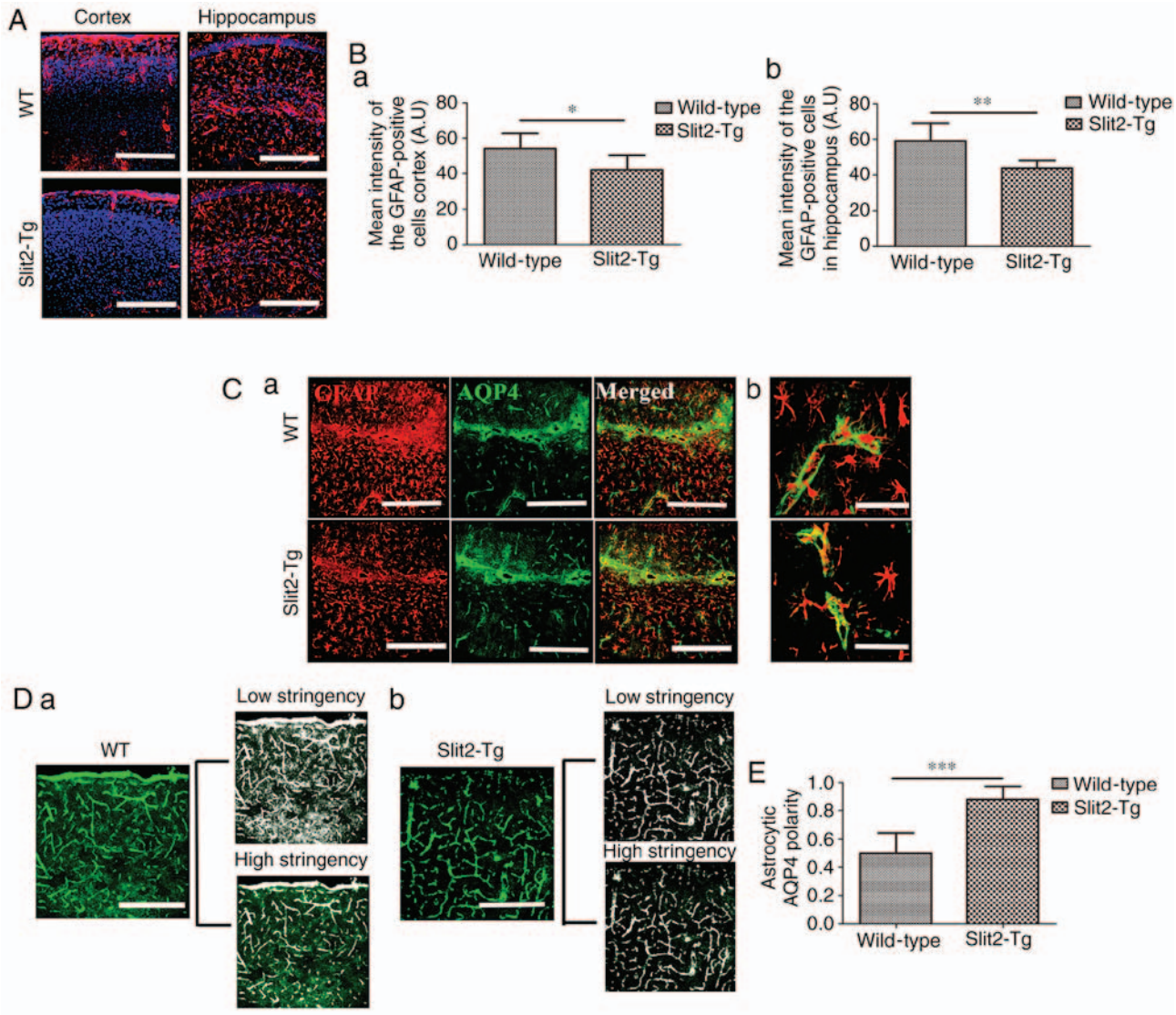

Figure 2. Slit2 inhibits reactivity of astrocytes and ameliorates AQP4 polarization in the aging mouse brain. The polarity of AQP4 and reactivity of astrocytes (GFAP-positive cells) was evaluated by immunofluorescence staining. (A) GFAP-positive cells were widespread in the cortex and hippocampus of the aging brains of Slit2-Tg and WT mice (magnification, x250; scale bar=250 μm). (B) Quantitative analysis of the mean pixel intensity of GFAP in the (a) cortex and (b) hippocampus. (C) Immunofluorescence (a) double-labeling of GFAP and AQP4 (magnification, x250; scale bar=250 μm) showed (b) expression of AQP4 distributed around the astrocytic endfeet, with less in the astrocytic soma in Slit2-Tg mice, whereas the opposite was observed in the WT mice (magnification, x750; scale bar=75 μM). (D) Low stringency images show all AQP4-immunoreactive pixels in the image, high stringency images captured all pixels around perivascular endfeet in (a) WT mice and (b) Slit2 mice (magnification, x250; scale bar=250 μm). (E) AQP4 polarity was derived as the ratio of low stringency:high stringency. Each value is expressed as the mean ± standard deviation. *P<0.05, **P<0.01 and ***P<0.001; n=6 per group). Slit2, slit guidance ligand 2; Tg, transgenic; WT, wild-type; GFAP, glial fibrillary acidic protein; AQP4, aquaporin-4.

increased at 60 min, compared with that at 5 min (t=0.276, P<0.001) in the aging WT mice, whereas the Wilcoxon rank sum test on the fluorescence intensity was significantly decreased at 60 min, compared with that at 5 min (P<0.001) in the aging Slit2-Tg mice. These results indicated that the overexpression of Slit2 accelerated paravascular CSF-ISF exchange in the aging brain.

Overexpression of Slit2 inhibits the reactivity of astrocytes and improves AQP4 polarity. The depolarization of AQP4 in reactive astrocytes is closely associated with impairment of the paravascular pathway in the aging brain (3). To understand why the overexpression of Slit2 restores the function of the paravascular pathway, the activation of astrocytes in the brain parenchyma and the polarization of AQP4 were evaluated. As shown in Fig. 2A, the GFAP-positive astrocytes were widespread in the cortex and hippocampus of the aging brain in WT and Slit2-Tg mice. An independent sample t-test indicated that the mean fluorescence intensity of GFAP-positive cells was significantly decreased in the Slit2-Tg mice, compared with that in the WT mice in the cortex (43.21±8.16, vs. 54.21±8.58; t=0.814, P<0.05; Fig. 2B-a) and hippocampus (40.02±4.28, vs. 59.08±9.89; t=0.069, P 0.01; Fig. 2B-b).

As a main component of water channel proteins expressed by astrocytes, AQP4 is polarized in the perivascular astrocytic endfeet in the healthy young brain, but not in the aging brain. AQP4 delocalization from the endfeet to the soma of astrocytes is, in part, associated with the failure of the paravascular pathway (3). Therefore, the present study investigated the polarization of AQP4 in the aging brain of WT and Slit2-Tg mice

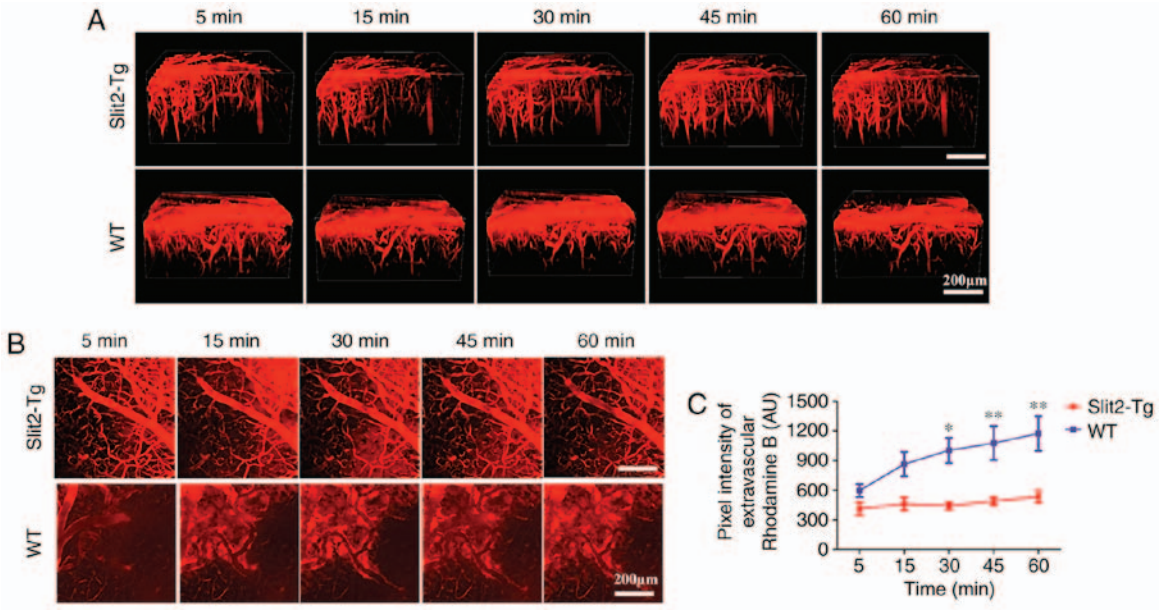

Figure 3. *In vivo* 2-photon imaging showing Slit2 maintains integrity of the BBB in aging mice. (A) 3D image stacks of the dynamic change of permeability of the BBB revealed by *in vivo* 2-photon microscopy following intravenous injection of dextran rhodamine B (red, 40 kDa). Magnification, x250; scale bar=200 μm. (B) Accumulation of rhodamine B around blood vessels of the brain parenchyma was evaluated by *in vivo* 2-photon microscopy (magnification, x250; scale bar=200 μm). (C) Quantitative analysis of the fluorescence intensity of rhodamine B. Each dataset is expressed as the mean ± standard deviation. (*P<0.05 and **P<0.01, vs. Slit-Tg; n=6 per group.). Slit2, slit guidance ligand 2; Tg, transgenic; WT, wild-type; BBB, blood-brain barrier

(Fig. 2C-a). In the Slit2-Tg mice, the expression of AQP4 was well distributed around the perivascular region, where AQP4 sheathed the astrocytic endfeet, and was less widespread in the astrocytic soma (Fig. 2C-b), whereas AQP4 was mis-located in the soma of astrocytes in the WT mice (Fig. 2C-b). According to a previous report (21), the value of AQP4 polarity was analyzed, which was defined as the low stringency area (overall area of AQP4-immunoreactivity in the image): High stringency area (area of intense AQP4-immoreactivty localized to the perivascular endfeet in the image) in the WT mice (Fig. 2D-a) and Slit2-Tg mice (Fig. 2D-b). An independent sample t-test indicated that astrocytic AQP4 polarity was significantly increased in the aging Slit2-Tg mice (0.88±0.10), compared with that in the WT mice (0.50±0.15; t=0.368, P<0.001, Fig. 2E). This result suggested that the improved paravascular pathway function in the aging brain induced by the overexpression of Slit2 was accomplished by the enhancement of astroglial water transport.

Overexpression of Slit2 maintains the integrity of the BBB in the aging brain. The disruption of the BBB caused by aging results in loss of vasomotion and decreases the efficiency of paravascular pathway clearance of Aβ (3,23), In the present study, the dynamic change of BBB function was evaluated by *in vivo* 2-photon microscopy and intravenous injection of dextran rhodamine B (MW 40 kDa). The 3D image stacks (Fig. 3A) showed that intravenous injection of dextran rhodamine B rapidly leaked from blood vessels into the brain parenchyma of WT mice. However, rhodamine B was restricted inside the blood vessels of the brain and minimal leakage was observed in the brain parenchyma of the Slit2-Tg mice.

To quantify the leakage of rhodamine B from the BBB, the total fluorescence intensity in the extravascular compartment was analyzed (24) (Fig. 3B). Two-way repeated ANOVA indicated no significant interaction between group and time factors (P>0.05). The main effect of the group and time factors were significant (F=4.152, P<0.05 and F=41.52, P<0.001, respectively). Bonfferoni's post hoc test was used to analyze the fluorescence intensity to examine the BBB permeability. No significant difference between the WT and Slit 2-Tg mice was observed at 5 min (598.50±162.11, vs. 414.41±153.84 AU, P>0.05) or 15 min (864.48±299.30, vs. 460.78±159.32 AU, P>0.05). The fluorescence intensity in the extravascular compartment was significantly decreased in the Slit-Tg mice, compared with that in the WT mice at 30 min (443.08±85.49, vs. 1,004.13±310.60 AU, P<0.05), 45 min (1,077.08±420.20, vs. 489.39±104.72 AU, P<0.01) and 60 min (1,174.16±427.65, vs. 536.12±148.46 AU, P<0.01) (Fig. 3C). These results indicated that the overexpression of Slit2 maintained the integrity of the BBB in the aging brain.

Overexpression of Slit2 reduces the accumulation of Aβ in the aging brain. The paravascular pathway and interstitial waste removal are suppressed with aging, which may contribute to the accumulation of Aβ leading to the pathogenesis of neurodegenerative diseases, including AD (3). To evaluate the effect of Slit2 on the accumulation of Aβ, immunofluorescent staining was performed to analyze the deposition of Aβ1-42 and Aβ1-40 in the brain parenchyma of aging mice. It was found that increased Aβ1-40 moved out from the blood vessels of the WT mice than that in the Slit2-Tg mice in the cortex and hippocampus (Fig. 4A). An independent sample t-test indicated that the overall fluorescence intensity was significantly decreased in the cortex of the Slit2-Tg mice (13.65±2.57), compared with that of the WT mice (33.70±8.18; t=5.726, P<0.001) (Fig. 4B). The accumulation of intra-neuronal Aβ1-42 was further analyzed in the two regions

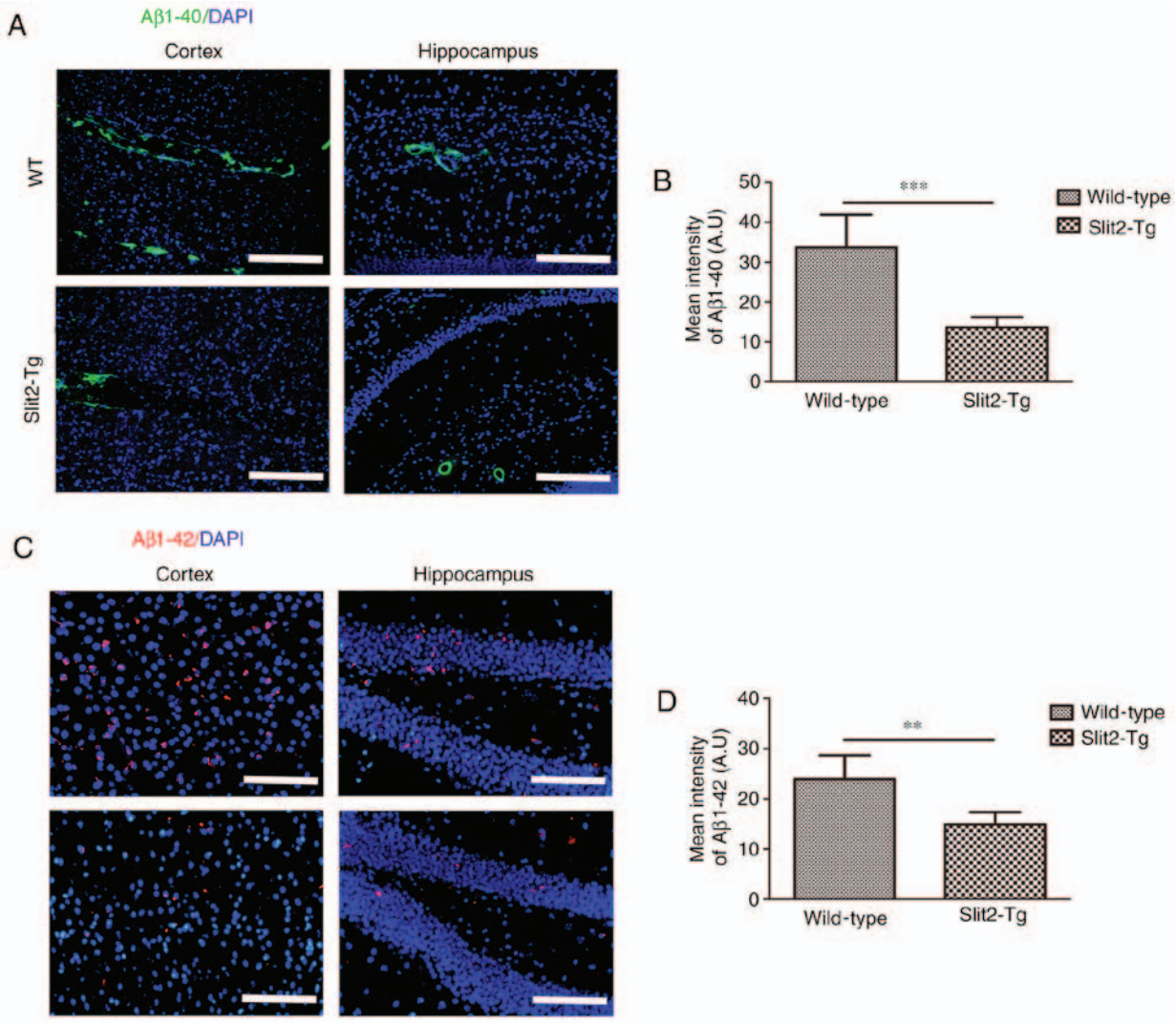

Figure 4. Slit2 decreases the deposition of Aβ in the brain parenchyma of aging mice. Expression of (A) Aβ1-40 (magnification, x100; scale bar=100 μm) in the cortex and hippocampus of the aging brain of Slit2-Tg and WT mice were evaluated by immunofluorescence staining. (B) Mean pixel intensity of Aβ1-40 the cortex. (C) Expression of Aβ1-42 (magnification, x200, scale bar=200 μm) in the cortex and hippocampus of the aging brain of Slit2-Tg and WT mice were evaluated by immunofluorescence staining. (D) Mean pixel intensity of Aβ1-42 in the cortex. Compared with WT mice, accumulation of Aβ1-40 in the peri-arterial space was significantly decreased in the aging brain parenchyma of Slit2-Tg mice (P<0.001). Compared with WT mice, deposition of Aβ1-42 surrounding nerve cells was significantly decreased in the aging brain parenchyma of Slit2-Tg mice (P<0.01). Each dataset is expressed as the mean ± standard deviation (**P<0.01 and ***P<0.001; n=6 per group). Slit2, slit guidance ligand 2; Tg, transgenic; WT, wild-type; Aβ, amyloid β.

(Fig. 4C), and the mean fluorescence intensity of Aβ1-42 was also significantly decreased in the cortex of the Slit2-Tg mice (14.88±2.47), compared with that of the WT mice (23.98±4.70; t=4.194, P<0.01) (Fig. 4D). These results indicated that the overexpression of Slit2 restored the function of the paravascular pathway and reduced Aβ deposition in the aging brain.

Overexpression of Slit2 improves the spatial memory cognition of aging mice. To investigate the effect of the overexpression of Slit2 on the spatial memory cognition of aging mice, Morris water maze tests were performed. As shown in Fig. 5A, the Wilcoxon rank sum test revealed no significant difference in the latency to reach platforms between the WT mice and Slit2-Tg mice (42.097±3.842, vs. 44.739±2.194; P>0.05) on day 1. The Kruskal-Wallis test showed that the latency on different training days was significantly different (P<0.001) in the WT group. The Bonferroni test showed that the latency on day 4 (20.593±1.800) and day 5 (18.499±3.238) was significantly decreased, compared with that on day 1 (P<0.001; P<0.001); the latency on day 5 was also significantly decreased, compared with that on day 2 (31.788±2.554) (P<0.05). However, the latency on day 3 (31.402±4.214) did not differ significantly from that on the other days (all P>0.05). In the Slit2-Tg mice, the Kruskal-Wallis test showed that the latencies on different training days were significantly different (P<0.001). The Bonferroni test was used to compare with the latency on day 1. The latency to reach the platform was significantly lower on day 2 (19.326±2.995; P<0.001), day 3 (15.780±3.102; P<0.001), day 4 (19.108±3.436; P<0.001) and day 5 (12.327±1.479, P<0.001), however, no significantly difference was observed among these consecutive 3 days. The latency was significantly decreased in the Slit2-Tg mice, compared with that in the WT mice on days 2 and 3 (t=3.166 and 2.985, P<0.01); whereas no significant differences were observed on days 4 and 5 between the two groups (t=0.383 and 1.734, P>0.05). In the probe trial (Fig. 5B), the independent

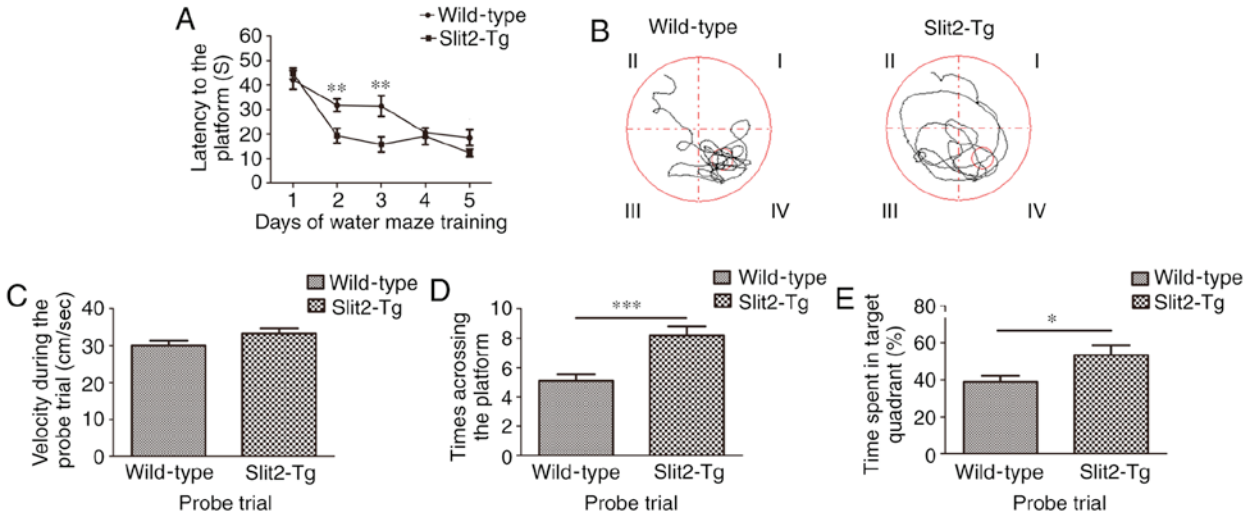

Figure 5. Slit2 improves the spatial memory cognition of aging mice. The spatial memory cognition of aging mice was evaluated using a Morris water maze. (A) Latency to reach the platform during Morris water maze training in WT and Slit2-Tg mice. (B) Representative swim paths of WT and Slit2-Tg mice in the trial. (C) Velocity of WT and Slit2-Tg mice during the trial. (D) Times to the target area (former platform) in WT and Slit2-Tg mice during the trial. (E) Time spent by WT and Slit2-Tg mice in the target quadrant during the trial. Each dataset is expressed as the mean ± standard error of the mean (*P<0.05, **P<0.01 and ***P<0.001; n=6 per group). Slit2, slit guidance ligand 2; Tg, transgenic; WT, wild-type.

sample t-test indicated no significant difference in velocities between the WT mice (30.03±1.30 cm/s) and Slit2-Tg mice (33.308±1.34 cm/s; t=1.753, P>0.05; Fig. 5C), whereas the time to the target area (previous platform) was significantly increased in the Slit2-Tg mice (8.20±0.59), compared with that in the WT mice (5.10±0.433; t=4.223, P<0.001; Fig. 5D). Finally, the time spent in the target quadrant (%) was analyzed (Fig. 5E), independent sample t-test indicated that the time spent in the target quadrant (%) was significantly increased in Slit2-Tg mice (53.417±5.287), compared with that in WT mice (38.982±3.215; t=2.333; P<0.05). These data collectively suggested that the overexpression of Slit2 restored the function of the paravascular pathway, which assisted in improving spatial memory cognition in the aging mice.

Discussion

The paravascular pathway has a 'glymphatic' role, responsible for water and waste exchange between the CSF and ISF, and the clearance of interstitial solutes in the brain (2,5,25). Dysfunction of the paravascular pathway has been linked to the accumulation of Aβ (26). Reactive astrogliosis and neuro-inflammation are prominent features of aging and the injured brain (3,18,27). Reactive astrocytes directly lead to a loss of paravascular astroglial AQP4 polarization from the endfeet to the soma, which is important in maintaining paravascular pathway function (3,28). Slit2 is widely expressed in various tissues, including the brain (29). During inflammation, Slit2 inhibits the secretion of certain inflammatory cytokines/chemokines, which is mediated by its Robo receptors (30,31). In neuroinflammation, cytokines have been shown to induce astrocyte activation (32); cytokines and chemokines produced by activated astrocytes further amplify inflammatory responses in the brain (33). Although, the way in which Slit2 reduces aging-related reactive gliosis remains to be fully elucidated, an early study indicated that Slit2 was expressed at a high level in GFAP-positive reactive astrocytes surrounding the necrotic tissue of the injured brain (34). Another study indicated that the administration of recombinant Slit2 reduces the neuroinflammation caused by brain injury (35). Therefore, the effect of Slit2 in improving paravascular pathway function in the aging brain may be associated with the inhibition of astrocyte activation by its anti-inflammatory property.

Substantial evidence had shown that Slit2 is important in promoting vascular stability by inhibiting endothelial hyperpermeability (31,36,37). Aging induces disruption of the BBB by increasing endothelial permeability. Disruption of the BBB results in loss of cerebrovascular contractile function through interacting with smooth muscle cells (38), and the impairment of vasomotion decreases the efficiency of paravascular pathway clearance of Aβ (23). In the present study, using transgenic mice overexpressing Slit2 in the brain, it was observed that the integrity of the BBB was maintained and the accumulation of Aβ was reduced in the brains of aging mice; these results were in accordance with the improved paravascular pathway found in the same transgenic aging mice. However, this result was unexpected, as homozygous Slit2-Tg mice with an intumescent head have been reported to show increased BBB permeability and Aβ deposition (10,15). This inconsistency may be due to differences in the methodology of previous studies, including the use of homozygous mice, and the use of Evans blue staining for assessment of the BBB and thioflavin staining for Aβ deposition. The abnormal phenotype in terms of development of the head was not observed in heterozygous transgenic mice in the present study, therefore, using heterozygous mice may avoid the negative effect of the transgene vector inserting randomly into the genome changing the expression of other genes. In addition, there are problems in using Evans blue as a marker for BBB leakage assessment, including residual dye in brain capillaries, binding of dye to plasma proteins and spectral shifts (39). In the present study, fluorescence-labeled dextrans were used for examination of the dynamic leakage of BBB under *in vivo* 2-photon microscopy, as labeled dextrans are considered more suitable for quantification in tissue (39).

In addition, Aβ deposition was detected using thioflavin staining in the previous study (15). Thioflavin staining is an easy and sensitive assay for amyloid. However, its lack of specificity for amyloid is a major drawback as it may react with several other proteins. In addition, the autofluorescence of granules, including elastin fibers and lipofuchsin, may increase the difficulty of data interpretation. Notably, in the previous study (15), thioflavin staining revealed marked Aβ deposition in the 9-month-old Tg2576 mice. Tg2576 mice are one of the widely used mouse models of AD, which overexpresses a mutant form of APP (isoform 695) with the Swedish mutation (KM670/671NL). This result is contradictory with general findings that increased Aβ levels and amyloid plaques in Tg2576 mice are evident at 11-13 months of age (40). By contrast, using specific antibodies for Aβ1-40 and Aβ1-42, the present study found that the accumulation of Aβ1-40 and Aβ1-42 was significantly decreased in the aging brains of Slit2-Tg mice. Aβ, a major component of senile plaques, has distinctive toxic effects on neurons and astrocytes. Aβ can induce reactive morphological changes and the upregulation of GFAP in astrocytes *in vitro* (41). In addition, cerebral amyloid angiopathy results in loss of the perivascular localization of AQP4 in mouse models and humans with AD (42). Therefore, in the present study, the decrease of Aβ deposition in the brains of Slit2-Tg mice was consistent with the inhibition of astroglial reactivity and maintenance of AQP4 polarity.

In conclusion, the overexpression of Slit2 in the aging brain improved the function of the paravascular pathway, maintained the integrity of the BBB, and decreased Aβ accumulation and age-related impaired spatial memory cognition. Further understanding of the mechanism underlying the function of Slit2 in the paravascular pathway of the aging brain may provide a novel strategy to reduce excess protein waste deposition and delay, or prevent the onset of neurodegenerative diseases.

Acknowledgements

Not applicable.

Funding

This study was supported by the National Natural Science Foundation of China [grant nos. 31472061, 31702074, 81371441, 81371255, 81572230 and 81671102] and the Guangdong Provincial Science & Technology Project [gran t nos. 2013B060300025, 2013B051000036, 2013B051000018, 2014B020212001, 2014A030304018 and 2014B040404053]. Funding sources had no involvement in the experimental design or interpretation of results.

Availability of data and materials

The datasets used and/or analysed during the current study are available from the corresponding author on reasonable request.

Authors' contributions

GL, XH, ZP, RH, YLa and YZ designed the experiments. XH, HL, YW, YG, SL, YLi and HJ performed the experiments. GL, XH, ZP, RH, LW and YZ analyzed the data. GL and XH and LW wrote the paper. RH and LW edited and revised the manuscript. YZ and YLa reviewed the manuscript. All authors read and approved the final manuscript.

Ethics approval and consent to participate

All animal experiments in the present study were approved by the Institutional Animal Care and Use Committee of Guangdong Laboratory Animals Monitoring Institute (IACUC no. 2015023). All procedures were performed in accordance with the AAALAC guidelines.

Patient consent for publication

Not applicable.

Competing interests

The authors declare that they have no competing interests.

References

1. Ross CA and Poirier MA: Protein aggregation and neurodegenerative disease. Nat Med 10 (Suppl): S10-S17, 2004.
2. Iliff JJ, Wang M, Liao Y, Plogg BA, Peng W, Gundersen GA, Benveniste H, Vates GE, Deane R, Goldman SA, *et al*: A paravascular pathway facilitates CSF flow through the brain parenchyma and the clearance of interstitial solutes, including amyloid beta. Sci Transl Med 4: 147ra111, 2012.
3. Kress BT, Iliff JJ, Xia M, Wang M, Wei HS, Zeppenfeld D, Xie L, Kang H, Xu Q, Liew JA, *et al*: Impairment of paravascular clearance pathways in the aging brain. Ann Neurol 76: 845-861, 2014.
4. Iliff JJ, Wang M, Zeppenfeld DM, Venkataraman A, Plog BA, Liao Y, Deane R and Nedergaard M: Cerebral arterial pulsation drives paravascular CSF-interstitial fluid exchange in the murine brain. J Neurosci 33: 18190-18199, 2013.
5. Iliff JJ, Lee H, Yu M, Feng T, Logan J, Nedergaard M and Benveniste H: Brain-wide pathway for waste clearance captured by contrast-enhanced MRI. J Clin Invest 123: 1299-1309, 2013.
6. Brose K, Bland KS, Wang KH, Arnott D, Henzel W, Goodman CS, Tessier-Lavigne M and Kidd T: Slit proteins bind Robo receptors and have an evolutionarily conserved role in repulsive axon guidance. Cell 96: 795-806, 1999.
7. Ypsilanti AR, Zagar Y and Chedotal A: Moving away from the midline: New developments for Slit and Robo. Development 137: 1939-1952, 2010.
8. Altay T, McLaughlin B, Wu JY, Park TS and Gidday JM: Slit modulates cerebrovascular inflammation and mediates neuroprotection against global cerebral ischemia. Exp Neurol 207: 186-194, 2007.
9. Park JH, Pak HJ, Riew TR, Shin YJ and Lee MY: Increased expression of Slit2 and its receptors Robo1 and Robo4 in reactive astrocytes of the rat hippocampus after transient forebrain ischemia. Brain Res 1634: 45-56, 2016.
10. Han HX and Geng JG: Over-expression of Slit2 induces vessel formation and changes blood vessel permeability in mouse brain. Acta Pharmacol Sin 32: 1327-1336, 2011.
11. Yuen DA and Robinson LA: Slit2-Robo signaling: A novel regulator of vascular injury. Curr Opin Nephrol Hypertens 22: 445-451, 2013.
12. Elahy M, Jackaman C, Mamo JC, Lam V, Dhaliwal SS, Giles C, Nelson D and Takechi R: Blood-brain barrier dysfunction developed during normal aging is associated with inflammation and loss of tight junctions but not with leukocyte recruitment. Immun Ageing 12: 2, 2015.
13. Gorlé N, Van Cauwenberghe C, Libert C and Vandenbroucke RE: The effect of aging on brain barriers and the consequences for Alzheimer's disease development. Mamm Genome 27: 407-420, 2016.

14. National Research Council (U.S.), Committee for the Update of the Guide for the Care and Use of Laboratory Animals, Institute for Laboratory Animal Research (U.S.) and National Academies Press (U.S.): Guide for the Care and Use of Laboratory Animals. National Academies Press, Washington, D.C., 2011.
15. Li JC, Han L, Wen YX, Yang YX, Li S, Li XS, Zhao CJ, Wang TY, Chen H, Liu Y, *et al*: Increased permeability of the blood-brain barrier and Alzheimer's disease-like alterations in slit-2 transgenic mice. J Alzheimers Dis 43: 535-548, 2015.
16. Livak KJ and Schmittgen TD: Analysis of relative gene expression data using real-time quantitative PCR and the 2(-Delta Delta C(T)) method. Methods 25: 402-408, 2001.
17. He XF, Lan Y, Zhang Q, Liu DX, Wang Q, Liang FY, Zeng JS, Xu GQ and Pei Z: Deferoxamine inhibits microglial activation, attenuates blood-brain barrier disruption, rescues dendritic damage and improves spatial memory in a mouse model of microhemorrhages. J Neurochem 138: 436-447, 2016.
18. Luo C, Yao X, Li J, He B, Liu Q, Ren H, Liang F, Li M, Lin H, Peng J, *et al*: Paravascular pathways contribute to vasculitis and neuroinflammation after subarachnoid hemorrhage independently of glymphatic control. Cell Death Dis 7: e2160, 2016.
19. Harvey CD, Coen P and Tank DW: Choice-specific sequences in parietal cortex during a virtual-navigation decision task. Nature 484: 62-68, 2012.
20. Ren Z, Iliff JJ, Yang L, Yang J, Chen X, Chen MJ, Giese RN, Wang B, Shi X and Nedergaard M: 'Hit & Run' model of closed-skull traumatic brain injury (TBI) reveals complex patterns of post-traumatic AQP4 dysregulation. J Cereb Blood Flow Metab 33: 834-845, 2013.
21. Wang M, Iliff JJ, Liao Y, Chen MJ, Shinseki MS, Venkataraman A, Cheung J, Wang W and Nedergaard M: Cognitive deficits and delayed neuronal loss in a mouse model of multiple microinfarcts. J Neurosci 32: 17948-17960, 2012.
22. Wu H, Wu T, Li M and Wang J: Efficacy of the lipid-soluble iron chelator 2,2'-dipyridyl against hemorrhagic brain injury. Neurobiol Dis 45: 388-394, 2012.
23. Di Marco LY, Farkas E, Martin C, Venneri A and Frangi AF: Is vasomotion in cerebral arteries impaired in Alzheimer's disease? J Alzheimers Dis 46: 35-53, 2015.
24. Nhan T, Burgess A, Cho EE, Stefanovic B, Lilge L and Hynynen K: Drug delivery to the brain by focused ultrasound induced blood-brain barrier disruption: Quantitative evaluation of enhanced permeability of cerebral vasculature using two-photon microscopy. J Control Release 172: 274-280, 2013.
25. Hladky SB and Barrand MA: Mechanisms of fluid movement into, through and out of the brain: Evaluation of the evidence. Fluids Barriers CNS 11: 26, 2014.
26. Bakker EN, Bacskai BJ, Arbel-Ornath M, Aldea R, Bedussi B, Morris AW, Weller RO and Carare RO: Lymphatic Clearance of the Brain: Perivascular, paravascular and significance for neurodegenerative diseases. Cell Mol Neurobiol 36: 181-194, 2016.
27. Iliff JJ, Chen MJ, Plog BA, Zeppenfeld DM, Soltero M, Yang L, Singh I, Deane R and Nedergaard M: Impairment of glymphatic pathway function promotes tau pathology after traumatic brain injury. J Neurosci 34: 16180-16193, 2014.
28. Verkman AS, Anderson MO and Papadopoulos MC: Aquaporins: Important but elusive drug targets. Nat Rev Drug Discov 13: 259-277, 2014.
29. Blockus H and Chedotal A: Slit-Robo signaling. Development 143: 3037-3044, 2016.
30. London NR and Li DY: Robo4-dependent Slit signaling stabilizes the vasculature during pathologic angiogenesis and cytokine storm. Curr Opin Hematol 18: 186-190, 2011.
31. Zhao H, Anand AR and Ganju RK: Slit2-Robo4 pathway modulates lipopolysaccharide-induced endothelial inflammation and its expression is dysregulated during endotoxemia. J Immunol 192: 385-393, 2014.
32. Pekny M, Pekna M, Messing A, Steinhäuser C, Lee JM, Parpura V, Hol EM, Sofroniew MV and Verkhratsky A: Astrocytes: A central element in neurological diseases. Acta Neuropathol 131: 323-345, 2016.
33. Farina C, Aloisi F and Meinl E: Astrocytes are active players in cerebral innate immunity. Trends Immunol 28: 138-145, 2007.
34. Hagino S, Iseki K, Mori T, Zhang Y, Hikake T, Yokoya S, Takeuchi M, Hasimoto H, Kikuchi S and Wanaka A: Slit and glypican-1 mRNAs are coexpressed in the reactive astrocytes of the injured adult brain. Glia 42: 130-138, 2003.
35. Sherchan P, Huang L, Wang Y, Akyol O, Tang J and Zhang JH: Recombinant Slit2 attenuates neuroinflammation after surgical brain injury by inhibiting peripheral immune cell infiltration via Robo1-srGAP1 pathway in a rat model. Neurobiol Dis 85: 164-173, 2016.
36. Jones CA, London NR, Chen H, Park KW, Sauvaget D, Stockton RA, Wythe JD, Suh W, Larrieu-Lahargue F, Mukouyama YS, *et al*: Robo4 stabilizes the vascular network by inhibiting pathologic angiogenesis and endothelial hyperpermeability. Nat Med 14: 448-453, 2008.
37. Jones CA, Nishiya N, London NR, Zhu W, Sorensen LK, Chan AC, Lim CJ, Chen H, Zhang Q, Schultz PG, *et al*: Slit2-Robo4 signalling promotes vascular stability by blocking Arf6 activity. Nat Cell Biol 11: 1325-1331, 2009.
38. Moody DM, Brown WR, Challa VR, Ghazi-Birry HS and Reboussin DM: Cerebral microvascular alterations in aging, leukoaraiosis, and Alzheimer's disease. Ann NY Acad Sci 826: 103-116, 1997.
39. Saunders NR, Dziegielewska KM, Møllgård K and Habgood MD: Markers for blood-brain barrier integrity: How appropriate is Evans blue in the twenty-first century and what are the alternatives? Front Neurosci 9: 385, 2015.
40. Deacon RMJ: APP-based transgenic models: The Tg2576 model. In: Animal Models of Dementia. De Deyn PP and Van Dam D (eds). Humana Press, Totowa, NJ, pp387-398, 2011.
41. Yang W, Wu Q, Yuan C, Gao J, Xiao M, Gu M, Ding J and Hu G: Aquaporin-4 mediates astrocyte response to beta-amyloid. Mol Cell Neurosci 49: 406-414, 2012.
42. Wilcock DM, Vitek MP and Colton CA: Vascular amyloid alters astrocytic water and potassium channels in mouse models and humans with Alzheimer's disease. Neuroscience 159: 1055-1069, 2009.